

# Gaia vbroad—the Spectral-Line Broadening, and Binariness

E. Hadad<sup>1</sup>, T. Mazeh<sup>1</sup>, S. Faigler<sup>1</sup> and A.G.A. Brown<sup>2</sup>

<sup>1</sup> School of Physics and Astronomy, Tel Aviv University, Tel Aviv, 6997801, Israel  
e-mail: eyalhadad@mail.tau.ac.il

<sup>2</sup> Leiden Observatory, Leiden University, Einsteinweg 55, 2333 CC Leiden, The Netherlands  
e-mail: brown@strw.leidenuniv.nl

December 18, 2024

## ABSTRACT

The *Gaia* DR3 catalog includes line-broadening measurements (*vbroad*) for 3 524 677 stars. We concentrate here on the low-mass main-sequence (MS) sub-sample of the catalog, with  $(G_{BP} - G_{RP})_0$  in the range of 1–1.6, which includes 81 371 sources. The colour-magnitude diagram of the sample displays two distinct strips, the brighter of which is probably mostly composed of unresolved binaries, with mass ratios close to unity. We show that the suspected binary sub-sample displays a larger *vbroad* distribution, which we attribute to the unresolved absorption lines of the two components of each binary. A similar effect is seen in the GALAH data.

**Key words.** binaries: spectroscopic – techniques: radial velocities – methods: statistical – catalogues

## 1. Introduction

The *Gaia* space mission (Gaia Collaboration et al. 2016) carries a spectrometer with intermediate resolving power,  $R \approx 11\,500$ , covering the 846–870 nm range, with the primary goal of measuring the radial velocity (RV) of the bright sources (Cropper et al. 2018),<sup>1</sup> down to magnitude  $G_{RVS} \sim 16$  (Katz et al. 2023). The spectroscopic pipeline (Sarotetti et al. 2018) also derives a line-broadening parameter that estimates the broadening of the absorption lines relative to the pertinent template, yielding for *Gaia* DR3 (Gaia Collaboration et al. 2023b) *vbroad* values of 3 524 677 sources (Frémat et al. 2023).<sup>2</sup>

Despite the relatively low resolution of the spectrograph, the *vbroad* values can be used to estimate the stellar rotational broadening (e.g., Gilhool & Blake 2019), as discussed by Frémat et al. (2023), which in turn can help estimate the stellar rotational period, in case we know the stellar radius (e.g., Kiman et al. 2024) and the rotational axis inclination. Stellar rotation was derived in the last years from the observed photometric modulation (e.g., McQuillan et al. 2014; Iwanek et al. 2024; Ramsay et al. 2024), utilizing large photometric surveys, carrying astrophysical information on the different types of stars (e.g., Buder et al. 2021; Xiang et al. 2022). The *vbroad* database is another independent avenue to obtain stellar rotation periods, albeit less accurate.

Another large sample of stellar broadening is included in the GALAH DR3 database (Buder et al. 2021), based on observations of the HERMES spectrometer mounted on the Anglo-Australian Telescope (ATT). The *vbroad*, given for 581 149 sources,<sup>3</sup> is one of its stellar parameters.

With HERMES, the AAT achieves a median spectral resolution of 28 000 to create a sample surpassing *Gaia*'s quality. HERMES covers a non-contiguous range of 1 000 Å, spanning across the blue (4 713–4 903 Å), green (5 648–5 873 Å), red (6 478–6 737 Å), and infrared (7 585–7 887 Å) wavelengths. *vbroad* is given for sources up to  $V \sim 20$ , 92% of which are brighter than  $V = 14$  (Barden et al. 2010; Heijmans et al. 2012; Farrell et al. 2014; Sheinis et al. 2015).

In this paper, we study the impact of the binarity of the main-sequence (MS) *Gaia* sources on the derived line width—*vbroad*. We identified the binaries by their brightness excess relative to their colour on the *Gaia* colour-magnitude diagram (CMD) (e.g., Donada et al. 2023; Wallace 2024). Kovalev et al. (2024, 2022) used a somewhat similar approach, identifying  $\sim 10^4$  double-lined spectroscopic binary (SB2) candidates in LAMOST spectra by their larger rotational velocity values.

Section 2 shows that the sample of late MS *Gaia* sources with derived *vbroad* values displays two strips. The upper strip is mostly composed of unresolved binaries with relatively luminous secondaries, displaying a significantly larger *vbroad* distribution. Section 3 repeats the analysis for a sample of stars with GALAH *vbroad*, showing similar results. Section 4 discusses and concludes our findings.

## 2. Identifying two CMD Strips in the late-type MS *Gaia* stars with *vbroad* measurements

Out of the original *vbroad* sample, which consists of 3 524 677 sources, we consider only sources with  $\varpi > 0$  and  $\sigma_\varpi/\varpi < 10\%$ , leaving 3 238 383 sources, from which we only consider those with given extinction coefficients, reducing our population size to 1 834 196.

To focus on the late MS stars of the sample, we consider

<sup>1</sup> <https://gea.esac.esa.int/archive/documentation/GDR3/index.html>

<sup>2</sup> <https://gea.esac.esa.int/archive/>

<sup>3</sup> <https://vizier.cds.unistra.fr/viz-bin/VizieR-3?-source=J/MNRAS/506/150/stars>

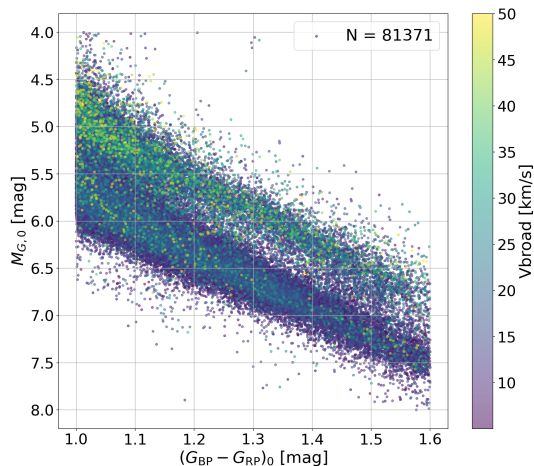


**Fig. 1.** Our vbroad sample, for sources with given extinction coefficients,  $\varpi > 0$ ,  $\sigma_\varpi/\varpi < 10\%$ ,  $(G_{BP} - G_{RP})_0 \in [1, 1.6]$  and  $M_{G,0} \in [4, 8]$ , colour-coded for vbroad. The 215 sources with vbroad well above 50 km/s are rounded to that value in the colour coding; of these, 204 are located on the upper strip.

a restricted sample of stars within an extinction-corrected colour of  $(G_{BP} - G_{RP})_0$  range of 1–1.6, and extinction-corrected absolute  $G$  magnitude ( $M_{G,0}$ ) of 4–8, leaving us with 81 371 stars, plotted in Fig. 1, colour-coded by the vbroad values. The diagram clearly displays two parallel strips, where the upper strip displays larger values of vbroad. This strip is probably composed of unresolved binaries (Freund et al. 2024; Phillips et al. 2024; Wallace 2024), which are more luminous than their primaries, due to the brightness contribution of their secondaries.

To show that this is indeed the case, we simulate the CMD location of binary systems at solar metallicity and age of 4.5 Gyr with different mass ratios, using the PARSEC<sup>4</sup> (e.g., Bressan et al. 2012; Chen et al. 2014; Tang et al. 2014; Marigo et al. 2017) tracks (see Fig. 1 of Wallace (2024)). Figure 2 seems to support the binary hypothesis, suggesting the upper strip is composed of unresolved binaries with  $q \gtrsim 0.7$ .

### 2.1. Separating the Binaries From the Single Stars

To identify the separation between the two populations, we split the  $(G_{BP} - G_{RP})_0$  range into six bins of 0.1 mag each and plot in Fig. 3 the  $M_{G,0}$  histogram in each bin. Each of the six histograms resembles a mixture of two Gaussians, corresponding to the lower and upper strips.

For each histogram, we fit a two Gaussians mixture<sup>5</sup> and define the separation between the two populations as the intersection of the two Gaussians. Table 1 lists for each  $(G_{BP} - G_{RP})_0$  bin the parameters of the two Gaussians and the  $M_{G,0}$  separation. Note that this splitting between single and binary stars is based only on their CMD location, ignoring their vbroad values.

Positioning the six points of separation in the middle of

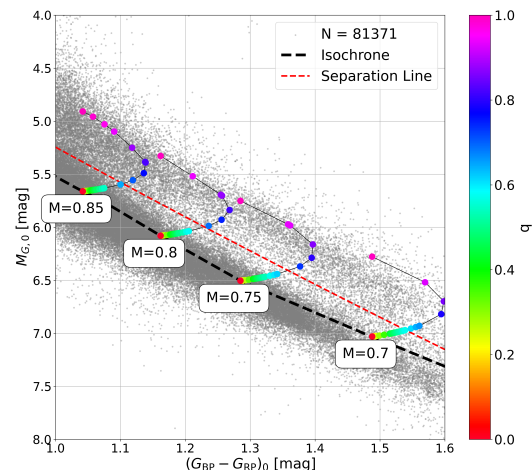


**Fig. 2.** Same as Fig 1, over-plotted with isochrones with an age of 4.5 Gyr and metallicity  $[\text{Fe}/\text{H}] = 0$ . Four primary masses (0.7, 0.75, 0.8 & 0.85 solar mass) are positioned on the isochrone. For each isochrone, binaries of different mass ratios are simulated and colour-coded by their mass ratio,  $q$ . The binaries with  $q = 1$  appear on the upper strip, positioned 0.752 magnitudes above their lower strip-single primaries. Isochrones are derived from the PARSEC models (see text). The red line is the separation between the two strips. The line equation is  $-0.44 \times x^2 + 4.3 \times x + 1.37$ . It is generated purely based on the  $M_{G,0}$  histograms, as explained in section 2.1. For a similar simulation, see Fig. 1 in Wallace (2024).

their respective bins, we fit a 2<sup>nd</sup>-degree polynomial that separates the two strips, as shown in Fig. 2.

The vbroad values of the two populations are displayed in Fig. 4 as a function of the  $M_{G,0}$  for the six colour bins. The figure distinctively shows a more extended vbroad distribution for the binaries. The different distributions are presented as violin plots in Fig. 5.

### 2.2. Comparison with Gaia DR3 MultipleStar Classifier

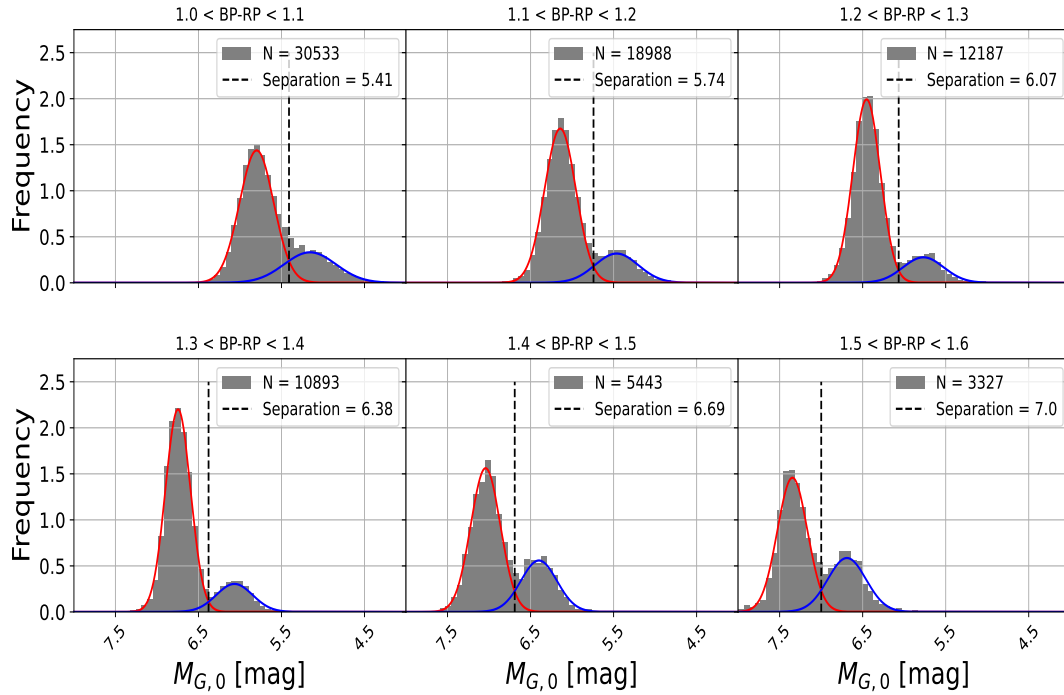
It is interesting to compare our binary identification against other indications of binarity. One such indicator is the multiple star classifier (MSC) of Gaia that infers stellar parameters for bright sources from the low-resolution BP/RP spectra and parallaxes, under the assumption that each of these sources is an unresolved coeval binary system. Their analysis resulted in a `logposterior_msc` parameter<sup>6</sup> that signifies how likely a system is a binary.

Table 2 compares the `logposterior` quartiles of the two strips, showing remarkably higher values, with higher probabilities of binarity, for the upper strip, supporting our conjecture.

<sup>4</sup> CMD 3.7: <http://stev.oapd.inaf.it/cgi-bin/cmd>

<sup>5</sup> <https://scikit-learn.org/stable/modules/generated/sklearn.mixture.GaussianMixture.html>

<sup>6</sup> [https://gea.esac.esa.int/archive/documentation/GDR3/Gaia\\_archive/chap\\_datamodel/sec\\_dm\\_astrophysical\\_parameter\\_tables/ssec\\_dm\\_astrophysical\\_parameters.html#astrophysical\\_parameters-logposterior\\_msc](https://gea.esac.esa.int/archive/documentation/GDR3/Gaia_archive/chap_datamodel/sec_dm_astrophysical_parameter_tables/ssec_dm_astrophysical_parameters.html#astrophysical_parameters-logposterior_msc)


**Fig. 3.** Histograms of  $M_{G,0}$  per  $(G_{BP} - G_{RP})_0$  bin.

**Table 1.** Coefficients of Gaussian Mixture

	Bin 1	Bin 2	Bin 3	Bin 4	Bin 5	Bin 6
Separation [mag]	5.41	5.74	6.07	6.38	6.69	7.0
1st Gaussian Mean [mag]	5.8	6.14	6.45	6.75	7.04	7.35
1st Gaussian std [mag]	0.04	0.04	0.03	0.02	0.03	0.03
2nd Gaussian mean [mag]	5.16	5.46	5.77	6.07	6.4	6.69
2nd Gaussian std [mag]	0.1	0.07	0.06	0.05	0.05	0.05
Difference between the Means [mag]	0.64	0.68	0.68	0.68	0.64	0.66

**Table 2.** Comparison of the logposterior binary indicator for the lower and upper stripe

	Lower Strip	Upper Strip
25 <sup>th</sup> percentile	-7573.17	430.42
50 <sup>th</sup> percentile	-4032.42	633.50
75 <sup>th</sup> percentile	-1513.59	729.08

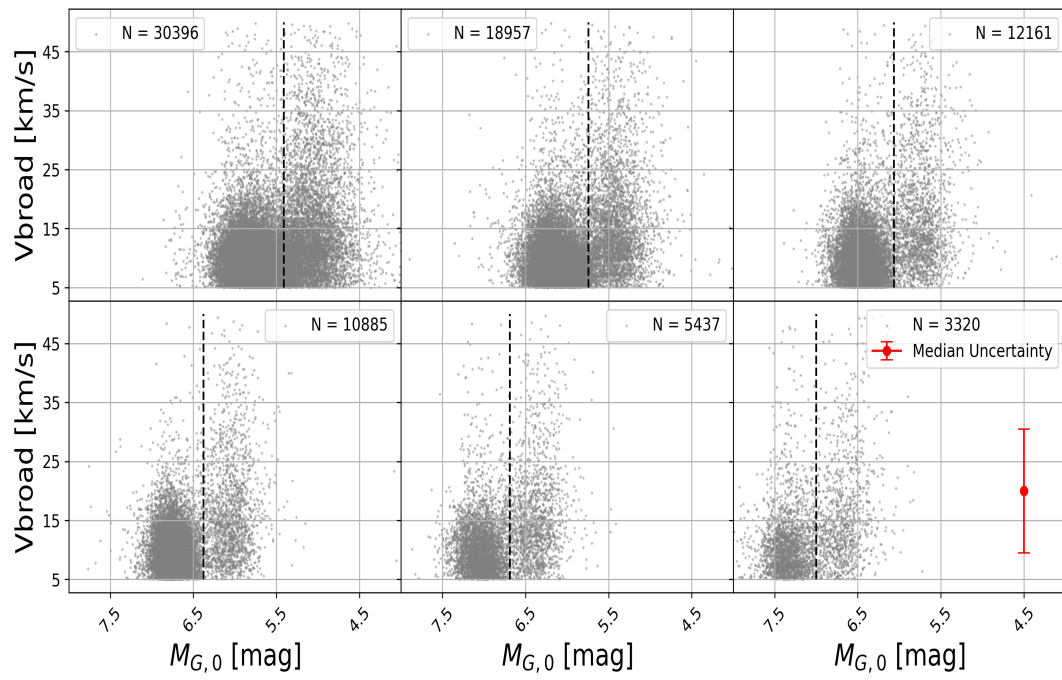


**Fig. 4.**  $V_{\text{broad}}$  vs.  $M_{G,0}$ . For visual clarity, only  $v_{\text{broad}} < 50$  km/s sources are shown. The bottom right panel shows an artificial point with the median uncertainty of the sample.



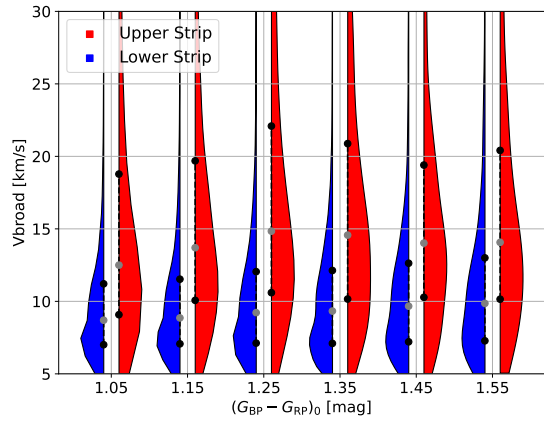


**Fig. 5.** Violin plot for the *Gaia* vbroad values, divided by colour bin and upper/lower strip. Vbroad is capped here at 30 km/s for visual clarity; the upper-strip distribution is elongated and extended toward higher vbroad values than the lower ones. Two black dots on each violin represent the 25th and 75th percentiles; the gray dots mark the median.

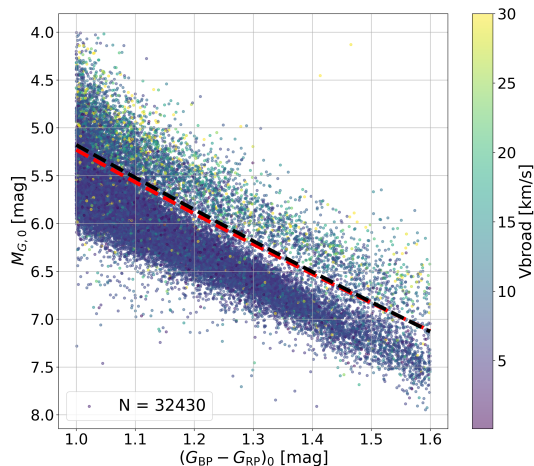


**Fig. 6.** Same as Fig. 1 for GALAH v<sub>broad</sub> population. The equation for the black line is  $y = -0.314 \times x^2 + 4.070 \times x + 1.422$ . The red line is the separation derived for the original population, over-plotted here for comparison. The 411 sources with v<sub>broad</sub> above 30 km/s were rounded to that value; of these, 242 are on the upper strip.

### 3. GALAH v<sub>broad</sub>

In this section, we apply our analysis to a different, more accurate, dataset of GALAH Buder et al. (2021), whose DR3 contains 588 571 sources; out of which, 588 464 have *Gaia* source\_id. After matching based on source\_id, we apply the same filters as described in Section 2:  $\varpi > 0$  and  $\sigma_\varpi/\varpi < 10\%$  brings us down to 422 785 stars. Now zooming into our two-strips area,  $(G_{BP} - G_{RP})_0 \in [1, 1.6]$  and  $M_{G,0} \in [4, 8]$ , leaves us with 32 675 sources. Out of those, 32 430 have GALAH’s v<sub>broad</sub> (4 529 of them also have *Gaia* v<sub>broad</sub>).

We choose to show only the main figures from the GALAH analysis. Figure 6 shows the two strips, over-plotted with GALAH separating line, together with the original *Gaia* line; the two are very similar. Figure 7 presents the violin plots, again showing close similarity to Figure 5. The logPosterior\_MSC analysis gave similar results.

#### 3.1. Example of GALAH spectra with different v<sub>broad</sub>

Figure 8 shows an example of four GALAH spectra of the H $\alpha$ -line region for sources with similar colour temperature (5 080–5 220 K, taken from teff\_gspphot<sup>7</sup>). Two of the sources, which are twice as bright as the other two, are suspected binaries, with v<sub>broad</sub> values that are much larger than those of the two single stars. One can see that the H $\alpha$ -line is split in those two spectra, for the ID=140314002601323 source in particular, consistent with the binary conjecture.

<sup>7</sup> [https://gea.esac.esa.int/archive/documentation/GDR3/Gaia\\_archive/chap\\_datamodel/sec\\_dm\\_main\\_source\\_catalogue/ssec\\_dm\\_gaia\\_source.html#gaia\\_source-](https://gea.esac.esa.int/archive/documentation/GDR3/Gaia_archive/chap_datamodel/sec_dm_main_source_catalogue/ssec_dm_gaia_source.html#gaia_source-)

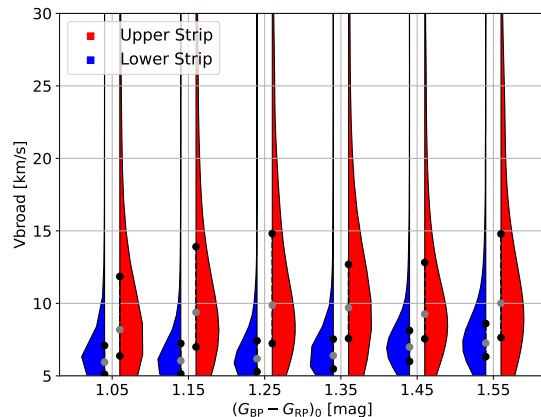


**Fig. 7.** Same as Fig. 5, for GALAH’s v<sub>broad</sub>. v<sub>broad</sub> is limited at 5–30 km/s for visual clarity. A similar trend is shown between the upper and lower strips. Two black dots are marked on each violin; they represent the 25th and 75th percentiles; the grey dot marks the median.

## 4. Discussion

This study considers 81 371 *Gaia* late-type MS sources with derived v<sub>broad</sub> values, the CMD of which displays a two-strip structure, as seen already by Freund et al. (2024), Phillips et al. (2024) and Wallace (2024). The objects in the upper strip, identified by their  $M_{G,0}$  excess, show a higher v<sub>broad</sub>-value distribution. Very similar behavior has been seen in the GALAH data.

We have shown that many of the upper strip stars are composed of unresolved binaries by simulating isochrones of binaries with different mass ratios. The simulations show that, regardless of the color, the upper strip includes binaries with mass ratios larger than about 0.7.

The v<sub>broad</sub> derivation is based on the *Gaia* RVS relatively low-resolution spectra, and therefore the v<sub>broad</sub> values are usually associated with large uncertainties (Frémat et al. 2023). Nevertheless, we were able to identify the binary effect on these values with high significance, because of the large number of sources available for the analysis.

We suggest that the larger v<sub>broad</sub> values of many of the unresolved binaries originate from the presence of the lines of the secondary star in the spectra of those binaries. The RV’s of the two components of the binary systems are separated by their orbital motion, but cannot be resolved by the RVS spectra. Therefore, the v<sub>broad</sub> pipeline measures a larger line width. Obviously, the RV difference between the two components depends on the orbital period and the binary inclination and phase at the time of each measurement, parameters that are not available. Nevertheless, the additional component induces an extra width to the line profile and consequently to the v<sub>broad</sub> estimation of the unresolved binaries.

The v<sub>broad</sub> excess of the unresolved binaries is on the order of 10 km/s. For a binary with a total mass of  $1M_\odot$ , a relative velocity of  $\sim 10$  km/s indicates an orbital period of  $\sim 30$  years and  $\sim 10$  au, assuming an orbital inclination close to  $90^\circ$ . Such a binary was impossible to detect as an astrometric binary in DR3 (e.g., Gaia Collaboration et al. 2023a), on the one hand, and cannot be resolved by *Gaia* (e.g., Castro-Ginard et al. 2024) on the other hand.

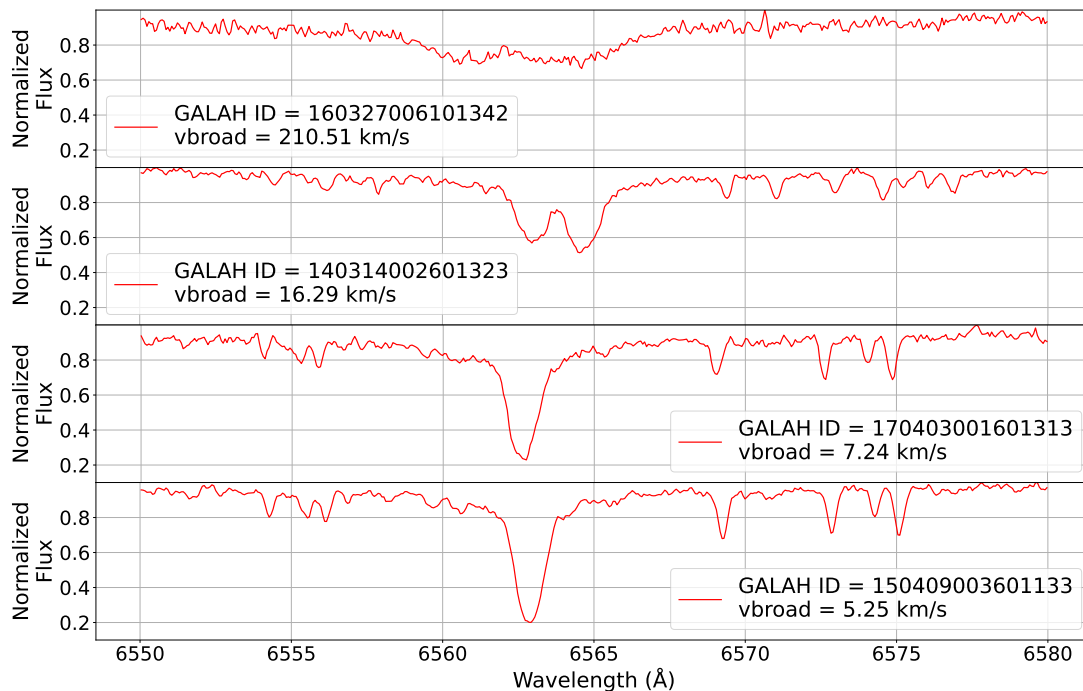


**Fig. 8.** GALAH spectra for four sources, two from the upper strip ( $M_{G,0} = 4.74$  for both) and two from the lower one, with a brightness of  $M_{G,0}$  of 5.49 and 5.50, respectively. The colour of the sources is  $(G_{BP} - G_{RP})_0 = 1.00$ – $1.01$ . The brighter sources show much broader absorption lines.

[Gaia Collaboration et al. \(2023a\)](#) classified 12% of the upper strip sources while only 4% of the lower strip sources as binaries, strengthening the suggestion about the high frequency of binarity in the upper strip.

We note that  $\sim 20\%$  of the *Gaia* and GALAH vbroad sources are on the upper strip. Assuming a high frequency of binaries in these upper strips is consistent with the estimation that about 50% of  $0.1$ – $1M_{\odot}$  stars are members of multiple-star systems (e.g., [Raghavan et al. 2010](#); [Duchêne & Kraus 2013](#); [Moe & Di Stefano 2017](#)), taking into account that only unresolved high mass-ratio binaries reside on the upper strip.

In the future, one will be able to detect an increasing number of these binaries as *Gaia* astrometric binaries, as the observational time span of the space mission increases. Further, with the TODCOR technique ([Zucker & Mazeh 1994](#)), one could try and identify the secondary spectrum in the RVS spectrum, like was done for the GALAH project ([Traven et al. 2020](#)), or in the *Gaia* BP/RP spectra ([Andrae et al. 2023](#)). These analyses will bring new opportunities for a better understanding of the true characteristics of the binary population of late-type stars.

*Acknowledgements.* We are indebted to the referee for thoughtful advice that significantly improved the previous version of the paper. This work has made use of data from the European Space Agency (ESA) mission *Gaia* (<https://www.cosmos.esa.int/gaia>), processed by the *Gaia* Data Processing and Analysis Consortium (DPAC, <https://www.cosmos.esa.int/web/gaia/dpac/consortium>). Funding for the DPAC has been provided by national institutions, in particular the institutions participating in the *Gaia* Multilateral Agreement. This work also made use of the Third Data Release of the GALAH Survey ([Buder et al. 2021](#)). The GALAH Survey is based on data ac-

quired through the Australian Astronomical Observatory, under programs: A/2013B/13 (The GALAH pilot survey); A/2014A/25, A/2015A/19, A/2017A/18 (The GALAH survey phase 1); A/2018A/18 (Open clusters with HERMES); A/2019A/1 (Hierarchical star formation in Ori OB1); A/2019A/15 (The GALAH survey phase 2); A/2015B/19, A/2016A/22, A/2016B/10, A/2017B/16, A/2018B/15 (The HERMES-TESS program); and A/2015A/3, A/2015B/1, A/2015B/19, A/2016A/22, A/2016B/12, A/2017A/14 (The HERMES K2-follow-up program). We acknowledge the traditional owners of the land on which the AAT stands, the Gamilaraay people, and pay our respects to elders past and present. This paper includes data that has been provided by AAO Data Central ([datacentral.org.au](http://datacentral.org.au)). We are indebted to the *Gaia* CU6 team that released the vbroad values for such a large sample, enabling this study.

## References

- Andrae, R., Fouesneau, M., Sordo, R., et al. 2023, *A&A*, 674, A27  
 Barden, S. C., Jones, D. J., Barnes, S. I., et al. 2010, in Society of Photo-Optical Instrumentation Engineers (SPIE) Conference Series, Vol. 7735, Ground-based and Airborne Instrumentation for Astronomy III, ed. I. S. McLean, S. K. Ramsay, & H. Takami, 773509  
 Bressan, A., Marigo, P., Girardi, L., et al. 2012, *MNRAS*, 427, 127  
 Buder, S., Sharma, S., Kos, J., et al. 2021, *MNRAS*, 506, 150  
 Castro-Ginard, A., Penoyre, Z., Casey, A. R., et al. 2024, *A&A*, 688, A1  
 Chen, Y. P., Trager, S. C., Peletier, R. F., et al. 2014, *The Messenger*, 158, 30  
 Cropper, M., Katz, D., Sartoretti, P., et al. 2018, *A&A*, 616, A5  
 Donada, J., Anders, F., Jordi, C., et al. 2023, *A&A*, 675, A89  
 Duchêne, G. & Kraus, A. 2013, *ARA&A*, 51, 269  
 Farrell, T. J., Birchall, M. N., Heald, R. W., et al. 2014, in Society of Photo-Optical Instrumentation Engineers (SPIE) Conference Series, Vol. 9152, Software and Cyberinfrastructure for Astronomy III, ed. G. Chiozzi & N. M. Radziwill, 915223  
 Frémat, Y., Royer, F., Marchal, O., et al. 2023, *A&A*, 674, A8  
 Freund, S., Czesla, S., Predehl, P., et al. 2024, arXiv e-prints, arXiv:2401.17282

- Gaia Collaboration, Arenou, F., Babusiaux, C., et al. 2023a, A&A, 674, A34
- Gaia Collaboration, Prusti, T., de Bruijne, J. H. J., et al. 2016, A&A, 595, A1
- Gaia Collaboration, Vallenari, A., Brown, A. G. A., et al. 2023b, A&A, 674, A1
- Gilhool, S. H. & Blake, C. H. 2019, ApJ, 875, 8
- Heijmans, J., Asplund, M., Barden, S., et al. 2012, in Society of Photo-Optical Instrumentation Engineers (SPIE) Conference Series, Vol. 8446, Ground-based and Airborne Instrumentation for Astronomy IV, ed. I. S. McLean, S. K. Ramsay, & H. Takami, 84460W
- Iwanek, P., Soszyński, I., Stępień, K., et al. 2024, Acta Astron., 74, 1
- Katz, D., Sartoretti, P., Guerrier, A., et al. 2023, A&A, 674, A5
- Kimani, R., Brandt, T. D., Faherty, J. K., & Popinchalk, M. 2024, AJ, 168, 126
- Kovalev, M., Chen, X., & Han, Z. 2022, MNRAS, 517, 356
- Kovalev, M., Zhou, Z., Chen, X., & Han, Z. 2024, MNRAS, 527, 521
- Marigo, P., Girardi, L., Bressan, A., et al. 2017, ApJ, 835, 77
- McQuillan, A., Mazeh, T., & Aigrain, S. 2014, ApJS, 211, 24
- Moe, M. & Di Stefano, R. 2017, ApJS, 230, 15
- Phillips, A., Kochanek, C. S., Jayasinghe, T., et al. 2024, MNRAS, 527, 5588
- Raghavan, D., McAlister, H. A., Henry, T. J., et al. 2010, ApJS, 190, 1
- Ramsay, G., Hakala, P., & Doyle, J. G. 2024, arXiv e-prints, arXiv:2407.07607
- Sartoretti, P., Katz, D., Cropper, M., et al. 2018, A&A, 616, A6
- Sheinis, A., Anguiano, B., Asplund, M., et al. 2015, Journal of Astronomical Telescopes, Instruments, and Systems, 1, 035002
- Tang, J., Bressan, A., Rosenfield, P., et al. 2014, MNRAS, 445, 4287
- Traven, G., Feltzing, S., Merle, T., et al. 2020, A&A, 638, A145
- Wallace, A. L. 2024, MNRAS, 527, 8718
- Xiang, M., Rix, H.-W., Ting, Y.-S., et al. 2022, A&A, 662, A66
- Zucker, S. & Mazeh, T. 1994, ApJ, 420, 806